PHYSICAL REVIEW B VOLUME 17, NUMBER 4 15 FEBRUARY 1978

# Transition-metal hydrides: Electronic structure and the heats of formation

C. D. Gelatt, Jr.
*Physics Department, Harvard University, Cambridge, Massachusetts 02138*

H. Ehrenreich and Jacquelyn A. Weiss
*Division of Applied Sciences, Harvard University, Cambridge, Massachusetts 02138*

(Received 23 June 1977)

Calculations of the electronic structure of transition-metal hydrides are applied to the cohesive energy of $3d$ and $4d$ monohydrides, and the single-particle lifetime of states in nonstoichiometric Cu and Pd hydrides. A simple formula is presented which delineates the principal contributions to the cohesive energy of the hydrides: (i) the formation of a metal-hydrogen bonding level derived of states of the pure metal band structure which have $s$ symmetry about the site of the added proton, (ii) a slight increase in binding of the metal $d$ bands due to the added attractive potential, and (iii) the addition of an extra electron to the metal electron sea. The calculations, corrected for Coulomb repulsion at the hydrogen sites, qualitatively reproduce the experimental trends of the heats of formation of the transition-metal hydrides. The single-particle lifetime calculations are in quantitative agreement with Dingle-temperature measurements and they correctly predict the existence of essentially undamped states on the hole sheets of the $\alpha$-phase PdH Fermi surface.

## I. INTRODUCTION

This paper discusses the systematics of the trends in the heats of formation for the $3d$ and $4d$ transition-metal hydrides. These are perhaps the simplest example of disordered interstitial metallic compounds in which one sublattice, corresponding to the metal, is ordered and the other sublattice, corresponding to the hydrogen, is disordered. The techniques developed for this purpose will be applicable to other systems generally containing appreciable vacancy concentrations such as many of the refractory compounds. Also discussed are the complex band structures of the nonstoichiometric, disordered, interstitial compounds. The results illustrate the evolution of the electronic level structure as hydrogen is added to the host metal.

The results for the heats of formation to be presented here put previous phenomenological models into perspective. These models are of three types: (i) the hydride-anion model[1] which is exemplified by the alkali hydrides such as LiH in which an electron is transferred from Li to H. Since LiH is an insulator, the general applicability of this model to the transition-metal hydrides is questionable; (ii) the covalent-hydrogen model[2] in which it is assumed that the hydrogen atoms are covalently bonded to the metal atoms; and (iii) the screened-proton model[3] in which the hydrogen enters the metal as a proton and contributes its electron to the unfilled states in the metal $d$ bands, the screening effects being treated within the Thomas-Fermi approximation. Because of its simplicity, this model has received considerable attention. However, screening effects are treated in an oversimplified fashion, and predictions, such as the existence of concentrated hydrides in the middle of the transition-metal rows correlated with peaks in the density of states,[4] are not consistent with the experimental situation. The present calculations indicate the formation of a metallic and largely nonionic bond between the metal and hydrogen, similar to that involving the $d$ electrons in pure transition metals. However, they are not inconsistent with the notion that some ionicity should be present on the left-hand side of each row.

Switendick[5] previously calculated the band structure of a large number of ordered transition-metal hydrides using the $X\alpha$ method.[6] The present calculations are based on the renormalized-atom approach,[7] a technique that has shown itself to be useful for the calculation of transition-metal cohesive energies[8] because it permits the ingredients contributing to binding to be delineated in a transparent physical fashion. The present band results are in substantial agreement with those of Switendick. None of the previous calculations, however, considered either complex energy bands of the nonstoichiometric hydrides or the heats of formation, which are the principal topics of this paper.

The complex energy bands are calculated using an extension of the average $t$-matrix approximation[9] to interstitial alloys. Detailed results are presented for $PdH_x$ as a function of hydrogen concentration. For small $x$ a discrete level is formed which lies below the palladium $d$-conduction-band complex.[10] This level is associated with the formation of a Pd-H bond. With increasing $x$ this level broadens into a band. The $d$ bands are substantially unaffected but shift slightly downward in energy, an effect which is important in stabilizing the hydride particularly when the *d* bands are appreciably filled. The upper conduction-band levels, which are unfilled except for the noble-metal hydrides, are depressed. States having wave functions with finite amplitude at the hydrogen site are broadened by the disorder with a width essentially proportional to the square of the amplitude. With increasing concentration the impurity band grows at the expense of the host band, in this case, portions of the conduction band. The calculations are in agreement with de Haas–van Alphen[11-13] and photoemission measurements[10] on $PdH_x$ and $CuH_x$.

The heats of formation are calculated for *stoichiometric* monohydrides placed on an NaCl lattice. The metal atoms are assumed to form a face-centered-cubic (fcc) configuration with the lattice constant chosen to yield the Wigner-Seitz radius of the pure metal. The detailed numerical results may be summarized by an empirical formula [cf. Eq. (4) below] which clearly delineates the contribution of three principal ingredients to the heat of formation: (a) the formation of the metal-hydrogen bonding band; (b) the downward shift of the *d* bands; and (c) the placement of the extra electron associated with the hydrogen at the Fermi energy. These one-electron results must, however, be modified to take into account the effects of Coulomb repulsion associated with the fact that more than one electron may be located on a hydrogen site. These Coulomb corrections are estimated within the framework of the Hubbard model.

The present results for stoichiometric monohydrides are expected to reflect the general trends of the heats of formation of hydrides over the entire concentration range for the following reasons. The complex band calculations for the nonstoichiometric hydrides indicate that the same physical effects contribute to the binding as in the stoichiometric case. In addition, Switendick's calculations[5] for ordered $Pd_4H$ show that the *d* shift is localized around the hydrogen atoms and will be roughly the same, per hydrogen atom, independent of the concentration. Except in the case of the noble metals, the contribution associated with placing the extra electron at the Fermi energy will be approximately independent of hydrogen concentration because of the large *d*-band density of states. The empirical formula may therefore be used to interpolate reasonably between the dilute and stoichiometric limits. Experimental determinations of the partial molal enthalpy of formation of nonstoichiometric hydrides also indicate that the heat of formation per gram atom of hydrogen varies slowly as a function of hydrogen concentration.[14] Finally, it should be noted that the strength of the binding is underestimated by considering monohydrides in place of polyhydrides, for those metals that form the latter.

While it is possible to perform the proper calculations for the nonstoichiometric case, the degree of complexity is much greater than is warranted for this preliminary survey and by the sparsity of available experimental information. The only systematic compilation of the strength of the metal-hydrogen bond covering the full 3*d* and 4*d* periods is that of the heat of solution of hydrogen at very great dilution. The calculated trends mirror the observed behavior. They show that on the left-hand side the hydride is most strongly bonded. The Coulomb corrections are also dominant in that part of the row. By contrast, on the right-hand side the heats of formation are largely endothermic and as a result the hydrides are unstable. In particular, the calculations account for the anomalous position of Pd in producing very weak bonding. (It is this feature that accounts for the usefulness of Pd as a catalyst.) The shape of the curve representing the heat of formation as a function of valence across the row is determined largely by the behavior of the Fermi energy as it traverses the *d* band. While the trends are satisfactorily explained for the 4*d* row, the agreement for the 3*d* row is somewhat less satisfactory, particularly as it pertains to the region around Co and Ni.

The general approach of this paper then is not so much to achieve results having quantitative accuracy, but rather to delineate the principal factors giving rise to the trends of the heats of formation and from these to deduce empirical relations that can be simply applied for predictive purposes. The relation developed here differs from those characterizing previous simpler theories in that it has been induced from detailed results based on a reasonable picture of the electronic energy-level structure rather than on intuitively appealing, but largely oversimplified models.

Section II is concerned with technical details involved in the band calculations. This discussion may be skipped by the reader interested only in the results, which are presented in Sec. III. Section IV is concerned with the calculation and discussion of the heats of formation for the 3*d* and 4*d* metal hydrides. A derivation of the averaged *t*-matrix approximation for a lattice with a basis is given in Appendix A. Appendix B discusses the accuracy of the calculated heats of formation.

## II. FORMAL MATTERS

While the transition metals and their hydrides form a variety of crystal structures,[1] for purposes of simplicity and intercomparison, the fcc structure has been assumed for the transition metals and the rocksalt structure for their hydrides. The extensively studied hydrides PdH and NiH have this structure. Experience indicates that the structure-independent contribution to the pure transition-metal cohesive energy is heavily predominant.[15] The same may be true for the hydrides. The replacement of polyhydrides by monohydrides (e.g., $TiH_2$ by TiH) implies that the calculations should underestimate the exothermic heat of formation per hydrogen atom.[16,17]

The metal potentials were generated by means of the renormalized-atom method[7] from free-atom $d^n s^1$ configuration Hartree-Fock wave functions.[18] This electronic configuration is nearly self-consistent with the $d$ and $s$ number count resulting from transition-metal band calculations[19] and leads to cohesive energies that agree well with experiment.[8] For the heat of formation calculations in Sec. IV, the renormalization radius for the metal sites, $R_0$, is chosen to be the pure-metal Wigner-Seitz radius for both the metal and the hydride. Since the renormalized-atom method assumes a full Wigner-Seitz correlation hole at each atomic site,[7] the neutral hydrogen renormalized-atom potential is simply that of a proton. As a result, it is unnecessary to define $R_0$ for hydrogen. However, it is still necessary to specify a hydrogen muffin-tin radius.

The choice of muffin-tin radii $R_{MT}$ for a lattice with a basis presents some difficulties. In the usual prescription for an fcc lattice, the metal spheres touch along the (110) direction to maximize sphere volume, leaving an octahedral sphere of radius $0.15a$ for the hydrogen atom. Switendick[5] has noted that the hydrogen atom is very poorly represented by such a small sphere since it accommodates only a fraction of the electronic charge of a hydrogen atom. As a reasonable alternative to metal "touching spheres" radii, Switendick suggests metal and hydrogen sphere radii which are respectively 65% and 35% of the metal-hydrogen separation. The resulting "65–35" radii reduce the metal-sphere volume by 28% and nearly double that of the hydrogen sphere. This choice, used here in the calculations for the nondilute hydrides, also reduces the discontinuity of the muffin-tin potential between the surfaces of the metal and hydrogen spheres by as much as 0.5 Ry. "Touching sphere" muffin-tin radii have been used in the case of the *dilute* nonstoichiometric hydrides (e.g., $PdH_x$ and $CuH_x$). The potential in the muffin-tin flat, $V_{MT}$, is taken to be the average of the metal potential in the region between $R_0$ and the "touching spheres" metal $R_{MT}$ in both the metal and hydride calculations.

The band structures for the transition metals and their stoichiometric hydrides were calculated using the symmetrized augmented-plane-wave (APW) method.[20] The nonstoichiometric hydrides were treated as a disordered alloy, with hydrogen atoms and vacancies randomly distributed on one of the fcc sublattices and metal atoms located on every site of the second sublattice. The complex band structures were obtained using the average $t$-matrix approximation [9](ATA) in conjunction with the Korringa-Kohn-Rostoker[21] (KKR) method as generalized to a lattice with a basis (see Appendix A and Ref. 17).

The Brillouin-zone integrations needed to obtain the sums of one-electron energies were computed by means of the method of special points in the Brillouin zone introduced by Baldereschi[22] and extended by Chadi and Cohen.[23] By using ten special points, this technique leads to Fermi energies and sums of one-electron energies of pure transition metals that are in good agreement with the corresponding quantities obtained from the Hodges's interpolation Hamiltonian.[17,24]

## III. COMPLEX ENERGY BANDS IN NONSTOICHIOMETRIC HYDRIDES

The modification of the metal band structure due to the addition of hydrogen to the interstitial sites of the lattice is qualitatively similar for all $3d$ and $4d$ transition metals.[25] Pd is used as an illustrative example here since Pd and PdH have been extensively studied experimentally.[26] The complex energy spectrum of disordered nonstoichiometric $PdH_x$ has not previously been obtained for the full range of hydrogen concentration. Earlier efforts have centered around stoichiometric PdH,[10] ordered $Pd_4H$ and $Pd_4H_3$,[5] and $PdH_x$ treated by the tight-binding coherent-potential approximation,[27] and the augmented-plane-wave virtual-crystal method.[27(a)]

Figure 1 shows the energy bands of $PdH_x$ calculated with a concentration-independent lattice constant $a = 7.32$ a.u. along the [100] and [111] directions for several values of the hydrogen concentration $x$ ranging between 0 and 1. The results for Pd and PdH [Figs. 1(a) and 1(e)] are in qualitative agreement with those of Mueller *et al.*[28] for Pd and Switendick[5] for PdH.[29] Comparison of the Pd and PdH band structures shows that: (i) the average energy of the lowest (valence) band in PdH is substantially lower than the lowest (valence) band in pure Pd; (ii) the unhybridized $d$

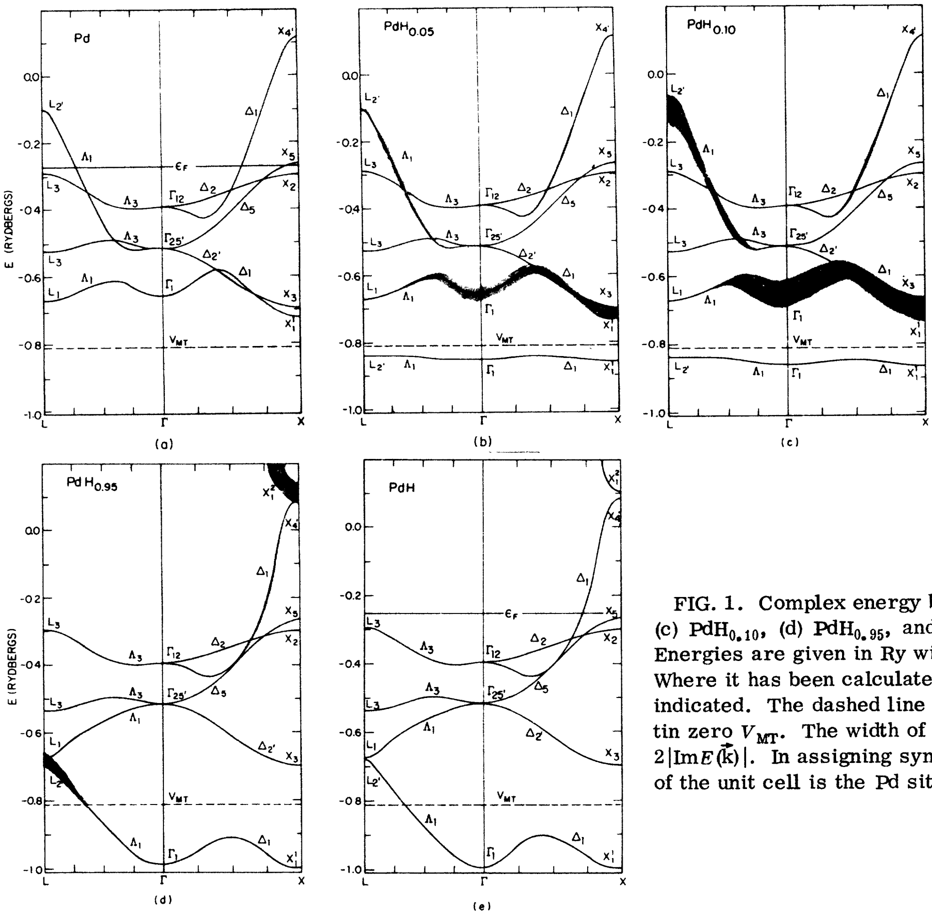

FIG. 1. Complex energy bands of (a) Pd, (b) $PdH_{0.05}$, (c) $PdH_{0.10}$, (d) $PdH_{0.95}$, and (e) PdH along $\Lambda$ and $\Delta$. Energies are given in Ry with respect to vacuum. Where it has been calculated, the Fermi energy $\epsilon_F$ is indicated. The dashed line corresponds to the muffin-tin zero $V_{MT}$. The width of the shading corresponds to $2|\mathrm{Im}E(\vec{k})|$. In assigning symmetry labels, the origin of the unit cell is the Pd site.

states are not markedly affected by hydride formation; (iii) conduction-band states such as those in the upper $\Delta_1$ band are shifted slightly downward in energy; and (iv) the state $X_1^2$, which lies above the $d$ bands in Pd [out of range in Fig. 1(a)], is 0.537 Ry lower in PdH.

Two features of particular interest in the nonstoichiometric alloys are the evolution of the lowest metal band into the lower-lying metal-hydride band and the damping of the states. Figs. 1(a) and 1(b) reveal two prominent changes in going from the pure metal to a hypothetical dilute hydride with 5 (at. %) hydrogen (beyond the $\alpha$-phase boundary of PdH). These are the appearance of a new hydrogenic level lying below the muffin-tin zero and the damping of the metal conduction states. [The damping is associated with the electronic lifetime due to scattering from the randomly occupied hydrogen sublattice, which is given by $-\pi^{-1}\,\mathrm{Im}E(\vec{k})$.] In Fig. 1 the width of the shading represents $2|\mathrm{Im}[E(\vec{k})]|$. Preliminary calculations[30] of the spectral density of nonstoichiometric $PdH_x$ demonstrate that $-\pi^{-1}\mathrm{Im}E(\vec{k})$ corresponds to the half-width of the peaks of the spectral density function $A(\vec{k},E)$, which are centered about $\mathrm{Re}E(\vec{k})$.

In the dilute limit, the flat impuritylike hydrogenic band [Fig. 1(b)] is not damped because within the ATA levels located below $V_{MT}$ have purely real energies. However, as the dispersion increases with increasing hydrogen concentration, the states in the vicinity of the point $L$ rise above $V_{MT}$ [Fig. 1(d)] and exhibit damping.

Figure 1(c) shows that the metal conduction states become more strongly damped with increasing $x$. For $x=0.95$ [Fig. 1(d)] the damping is so large and the associated spectral weight so small that these states can no longer be found numerically. As the spectral weight of the conduction states decreases, that associated with the states in the hydrogenic level becomes larger, until at $x=1$ the metal conduction states are replaced by the lower-lying metal-hydride band. We note that for intermediate $x$ neither of the two bands in question has full spectral weight and hence each contains less than two electrons.

The panels of Fig. 1 show that electronic states having different symmetries are differently affected by the disordered H sublattice. For the

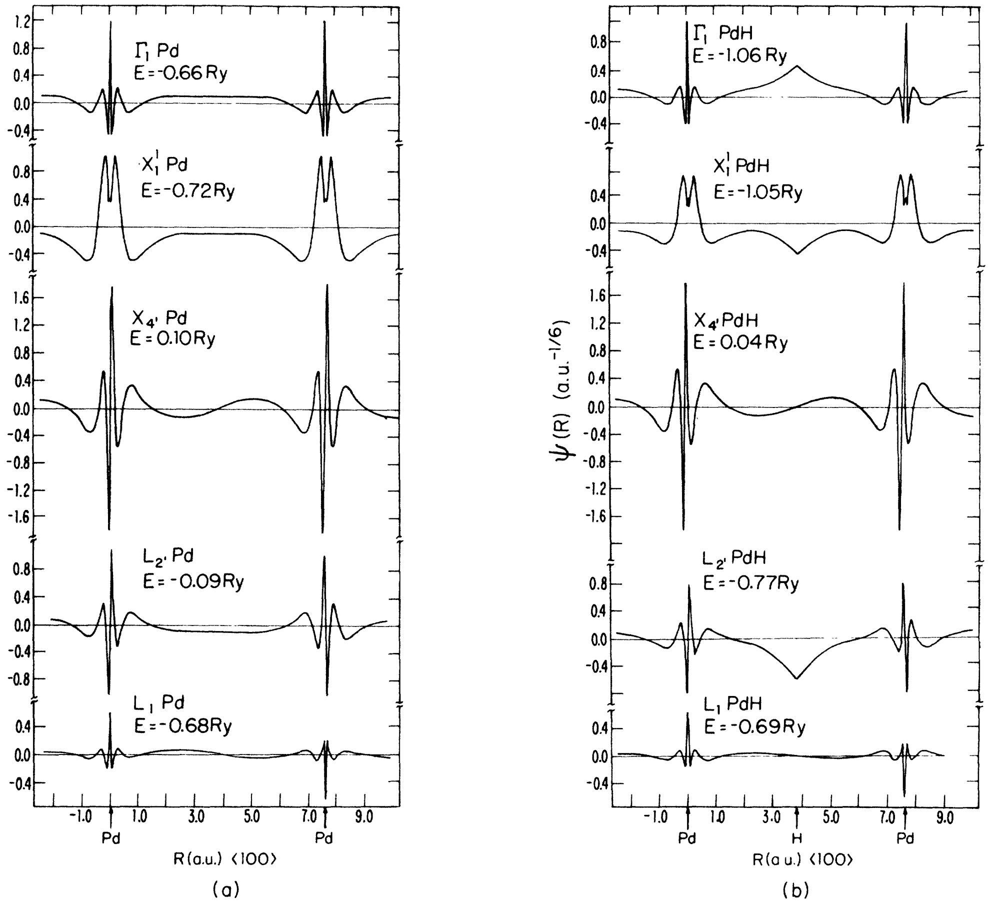

(a) (b)

FIG. 2. (a) Pd and (b) PdH wave functions along the [100] direction for the symmetry states $\Gamma_1$, $X_1^1$, $X_{4'}$, $L_{2'}$, and $L_1$. The label refers to the symmetry about the metal atom.

ordered hydrides, Switendick[5] has noted that only states having *s* symmetry about the proton are shifted appreciably. Typical of these at high-symmetry points are $\Gamma_1$, $X_1$, and $L_{2'}$ (denoting the state by its symmetry about the metal site). Wave functions for these states in Pd and PdH along the [100] direction are shown in Fig. 2. (The lattice constant for β-phase PdH, $a = 7.62$ a.u.,[26] has been used for both.) The wave functions of these states in Pd are seen to have finite amplitude in the vicinity of the interstitial site. This amplitude is increased in PdH and resembles that associated with a H 1*s* state. On the other hand, the $X_{4'}$ and $L_1$ wave functions, also shown in Fig. 2, exhibit a node, consistent with their *p* character about the interstitial site, in both Pd and PdH. Referring to Fig. 1, we note that the former states are strongly shifted and damped (in the nonstoichiometric hydride), whereas the latter remain relatively unaffected by the hydrogen alloying. The unhybridized *d* states are also affected only slightly. The damping of various states can also be shown to correlate well with the fraction of the charge of the state with *s* symmetry about the center of the octahedral hole of the pure metal lattice.[17]

The concentration dependence of the damping for the two types of states is illustrated in Fig. 3. For those having *s* symmetry about the interstitial site (e.g., $\Gamma_1, X_1, L_{2'}$), the damping increases monotonically over the concentration range ($x \lesssim 0.2$) that could be numerically explored. For the others (e.g., $X_{4'}$, $L_1$) the damping is far smaller and can be calculated over the entire concentration range. In the latter case, the damping is essentially parabolic in $x$ increasing until $x \cong 0.5$, then decreasing again as electrons scatter from smaller concentrations of H vacancies.

A second-order perturbation estimate can be used to obtain insight into the magnitude and sign of the metal band energy shifts resulting from the introduction of the hydrogen perturbing potential $V_H(r) = -2/r - V_{MT}$ into the octahedral sites of the lattice. The energy shift for dilute concentra-

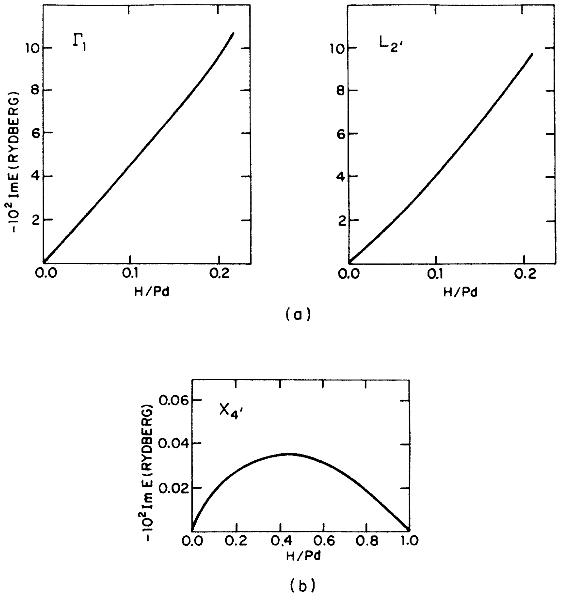

FIG. 3. $-\mathrm{Im}\,E(\vec{k})$ (Ry) for the states (a) $\Gamma_1$ and $L_{2'}$, and (b) $X_{4'}$ plotted against hydrogen concentration. Note the compressed concentration scale for the $X_{4'}$ panel.

tions $x$ is given approximately by

$$\Delta E_i(x) = x \int \psi_M^{i*}(r) V_{\mathrm{H}}(r) \psi_M^i(r) d^3r + x(1-x) \frac{|\int \psi_M^{i*}(r) V_{\mathrm{H}}(r) \psi_{\mathrm{H}}(r) d^3r|^2}{E_i - E_{\mathrm{H}}}, \tag{1}$$

where $\psi_M^i$ and $E_i$ are the metal wave function and energy corresponding to the state $i$, $\psi_{\mathrm{H}}$ is a hydrogenic wave function, $E_{\mathrm{H}}$ is the associated energy (−0.842 Ry in dilute PdH), and the integrals extend over the octahedral muffin-tin sphere. The first term represents an energy lowering due to the presence of the attractive hydrogen potential and the second a repulsion between the metal and hydrogenic states. The factors involving $x$ result from configuration averaging.

To evaluate the integrals, $\psi_M^i(r)$ is approximated as $(n_{\mathrm{oct}}^i / \frac{4}{3}\pi R_{\mathrm{H}}^3)^{1/2}$, where $n_{\mathrm{oct}}^i$ is the amount of Pd charge associated with the state $i$ in the octahedral sphere of radius $R_{\mathrm{H}}$, and $\psi_{\mathrm{H}}(r) \propto n_{\mathrm{H}}^{1/2} e^{-r}$, the normalization being chosen such that $\int |\psi_{\mathrm{H}}(r)|^2 d^3r = n_{\mathrm{H}}$, the charge due to the hydrogen level contained in the octahedral sphere.

The results are showh in Table I, which gives values of $n_{\mathrm{oct}}^i$ for $X_1^1$, $X_1^2$, $X_{4'}$, and $L_{2'}$ $(x = 0.05)$, the estimates of $\Delta E_i$, and the calculated values. The estimates predict the sign of the energy shifts correctly. For states lying far above $E_{\mathrm{H}}$ ($X_{4'}$, $X_1$, $L_{2'}$), $\Delta E_i$ is negative. The first-order term dominates since the repulsive interaction is small due to the large energy denominator in the second term of Eq. (1). For levels lying closer to $E_{\mathrm{H}}$ the repulsive term dominates and $\Delta E_i$ is positive. More generally, the higher-lying states are lowered with increased hydrogen concentration, whereas lower-lying states are raised.

The magnitude of the damping of the states in the lowest metal band in the hydride can be estimated with the help of the sum rules for the imaginary part of the self-energy $\Sigma(\vec{k}, E)$ derived by Velicky *et al.*[31] for a single-band model. A measure of the strength of the scattering in the single-band case is $\alpha \equiv x(1-x)\delta^2/\mu_2^{(0)}$, where $\delta$ and $\mu_2^{(0)}$, second moment of the unperturbed density of states, are defined by Eqs. (3.7) and (3.27) in Ref. 31. Approximating the density of states of the lowest band in the metal by a semicircular band of width $\Delta E = 0.2$ Ry, and taking $\delta$ to be the difference between the center of gravity of the lowest metal band and the hydrogen level ($\delta = 0.2$ Ry), one finds $\alpha = 0.2$ for $x = 0.05$, which lies within the virtual crystal region ($\alpha \ll 1$). In that case, the self-energy sum rule[31] implies

$$\Delta E \langle \mathrm{Im}\Sigma \rangle \approx \int \mathrm{Im}\Sigma(E + i0)\, dE = -\pi x(1-x)\delta^2.$$

TABLE I. Comparison of the $\mathrm{PdH}_{0.05}$ energy shifts of $X_1^1$, $X_1^2$, $X_{4'}$, and $L_{2'}$ as obtained from a perturbation estimate (third column) and the band calculation (fourth column). All energies are in Rydbergs. The number of Pd electrons contained in the octahedral sphere associated with each state $i$, $n_{\mathrm{oct}}^i$, is given in the first column. Calculated using the touching spheres muffin-tin radii, and the lattice constant of pure Pd ($a = 7.321$ a.u.).

| State | $n_{\mathrm{oct}}^i$ | $E_i$ (metal) (relative to atomic zero) | $\Delta E_i$ $(x = 0.05)$ (perturbation estimate) | $\Delta E_i$ $(x = 0.05)$ (band-calculation result) |
|---|---|---|---|---|
| $X_1^1$ | 0.053 | −0.720 | +0.025 | +0.008 |
| $X_1^2$ | 0.108 | 0.640 | −0.006 | −0.004 |
| $X_{4'}$ | 0.107 | 0.120 | −0.001 | −0.002 |
| $L_{2'}$ | 0.116 | −0.099 | −0.001 | −0.003 |

This predicts $\langle \mathrm{Im}\Sigma\rangle = -0.03$ Ry as compared with the KKR-ATA result $\langle \mathrm{Im}\Sigma\rangle \approx -0.02$ Ry. The split-band limit, which should underestimate the damping in the present case, predicts that the average value of $\mathrm{Im}\Sigma$ over the metal subband is $-0.008$ Ry.

The damping of the states on the Fermi surface can be measured in de Haas–van Alphen experiments. The Dingle temperature $T_D$ for a particular orbit is related to the average Fermi-surface damping of that orbit by $\langle \mathrm{Im}E\rangle = -\pi k_B T_D$. The calculated anisotropy of the belly orbit damping in $\mathrm{PdH}_x$ and $\mathrm{CuH}_x$ is shown in Fig. 4. The curves for the two materials are similar. The greatest damping occurs near the [111] direction where the metal Fermi-surface electrons have significant $s$-like character about the hydrogen site. The magnitude of the damping is larger for $\mathrm{CuH}_x$ because the Fermi level lies higher in the conduction band and the admixture of $s$ character about the hydrogen is greater. The ratio of the damping in the [110] direction to that in the [100] direction is greater than one for $\mathrm{CuH}_x$, while for $\mathrm{PdH}_x$ it is less than one. For states along [100], the higher the Fermi energy the smaller the damping because the states become less $s$-like as they approach $X_{4'}$, which has pure $p$ character about the hydrogen site. There is no similar symmetry restriction for the zone-boundary state along [110]. The higher Fermi energy in Cu thus leads to the observed damping ratio.

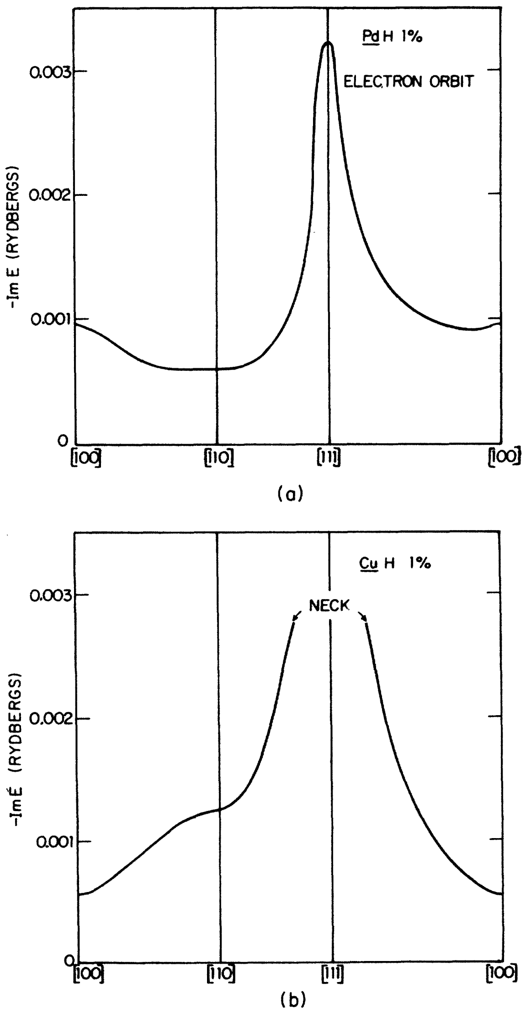

FIG. 4. Anisotropy of the Fermi-surface damping for (a) $\mathrm{PdH}_{0.01}$ (electron orbit), and (b) $\mathrm{CuH}_{0.01}$.

The Pd Fermi surface also contains $d$-band hole pockets centered at $X$ and $L$, and the open "jungle-gym" orbit. The damping of these states, which have almost pure metal $d$ character, is too small to determine (<0.0001 Ry) for 5% hydrogen content. As was predicted on the basis of these calculations,[13] the de Haas–van Alphen signal from the hole orbits can be measured experimentally in samples with as much as 3% hydrogen, the limit of $\alpha$-phase stability.[11]

The Fermi-surface damping in $\mathrm{CuH}_x$ has been investigated by Lengeler and Wampler,[12] who loaded Cu samples with several hundred parts per million of hydrogen. The calculated Dingle temperatures for several orbits[32] are compared with experiment in Table II.[33] The measured damping anisotropy for $\mathrm{CuH}_x$ is in excellent agreement with the results in Fig. 4(b). Measurements of the damping on the belly orbits of Pd have not been carried out to our knowledge.

Experimental information relevant to other physical features emerging from the present band calculations is relatively sparse. Eastman and co-workers[10] have observed a low-lying peak in photoemission studies of $\beta$-phase PdH. This band was found to lie 5.4 eV below the Fermi energy and to have a width of about 3 eV. The present calculations, which yield 8.2 and 3 eV for these quantities, are in reasonable agreement. Additional experiments performed on Ti indicate[34] that the hydrogen level found in the dilute limit broadens into a band as the hydrogen concentration is increased. This is consistent with the concentration-dependent broadening of the hydrogenic level shown in panels (b)–(e) of Fig. 1.

TABLE II. Average damping (in units of $10^{-3}$ Ry) per percent hydrogen for several orbits on the Cu Fermi surface. The experimental values are from Ref. 33.

| Orbit | Experiment | Theory |
|---|---|---|
| Neck | $2.25 \pm 0.12$ | 2.3 |
| ⟨100⟩ belly | $0.76 \pm 0.06$ | 0.84 |
| Dog's bone | $1.53 \pm 0.14$ | 1.43 |

TABLE III. Average energy of each band in Pd (first column) and PdH (second column). The difference (PdH average energy-Pd average energy) is indicated in the third column. The band energies are in Rydbergs and given with respect to vacuum. The number of *d* and non-*d* electrons per band contained in the metal muffin-tin sphere of Pd (first column) and PdH (second column). The PdH-Pd charge difference is indicated in the third column. All columns are for the Pd and PdH calculations of Fig. 1.

| | Average band energy | | | Metal *d* charge per band | | | Metal non-*d* charge per band | | |
|---|---|---|---|---|---|---|---|---|---|
| Band | Pd | PdH | Difference | Pd | PdH | Difference | Pd | PdH | Difference |
| 1 | −0.627 | −0.950 | −0.323 | 1.49 | 0.46 | −1.03 | 0.12 | 0.25 | 0.13 |
| 2 | −0.575 | −0.616 | −0.041 | 1.58 | 1.60 | 0.02 | 0.09 | 0.07 | −0.02 |
| 3 | −0.474 | −0.496 | −0.022 | 1.68 | 1.65 | −0.03 | 0.08 | 0.09 | 0.01 |
| 4 | −0.421 | −0.456 | −0.035 | 1.74 | 1.79 | 0.05 | 0.07 | 0.03 | −0.04 |
| 5 | −0.339 | −0.348 | −0.009 | 1.86 | 1.91 | 0.05 | 0.04 | 0.01 | −0.03 |
| 6 | −0.011 | −0.231 | −0.220 | 0.73 | 1.56 | 0.83 | 0.58 | 0.08 | −0.50 |

In connection with the hydride heats of formation to be considered in Sec. IV, it is useful to compare the average over the Brillouin zone of the energies of the pure metal and stoichiometric hydride bands. These average energies for Pd and their shifts (PdH average energy)-(Pd average energy), calculated by using ten special points,[23] are given in Table III. The most conspicuous changes occur in the lowest valence band (band 1) and the *d*-hybridized conduction states composing band 6.

These energy shifts are associated with changes in the metal charge distribution. Table III shows the amount of *d* and non-*d* charge contained in the metal muffin-tin sphere for each band in Pd and PdH and the difference (PdH charge minus Pd charge). As is apparent, the lowest Pd band (band 1) is a *d* band with a small amount of conduction-band character. The next four higher bands are substantially unhybridized *d* bands, while band 6 is a *d*-hybridized conduction band with much greater conduction character than band 1. In PdH, the *d* admixture of band 1 is reduced by approximately one electron with respect to band 1 of Pd. The charge decomposition of the *d* bands 2–5 is essentially unaltered. The *d* admixture of band 6 increases by nearly one *d* electron over the Pd value.

To understand these changes, we note that, because band 1 lies 0.24 Ry further below the *d* bands in PdH than in Pd, the *s*-*d* hybridization is reduced and the number of *d* electrons in that band is diminished. The missing charge (the sum of the metal *d* and non-*d* charges is less than 2) is located in the intersphere volume and in the hydrogen muffin-tin sphere and gives rise to the molecular Pd-H bond characterizing band 1 of the hydride. The increased *d* character of band 6 in PdH is due to the fact that the high-lying conduction states are brought, on the average, 0.2 Ry closer to the *d* bands, thereby increasing the *s*-*d* hybridization.

The much smaller energy shift of bands 2–5 is associated with weak *s*-*d* hybridization and small wave-function amplitude at the hydrogen sites. States at points of low symmetry in the Brillouin zone contain a non-negligible *s* admixture which results in an energy lowering in the hydride proportional to the amount of *s* admixture. Thus, the states in band 3 are shifted more than those in band 5 in accordance with the relative amounts of non-*d* charge. These shifts have not, to our knowledge, been discussed previously. Although small, they play an important role in hydride formation to be discussed in Sec. IV.

## IV. HEATS OF FORMATION OF STOICHIOMETRIC MONOHYDRIDES

The heat of formation per unit cell $\Delta E$ is defined by the reaction of metal $M$ with hydrogen gas to form the hydride $MH_x$:

$$M(\text{solid}) + \tfrac{1}{2}xH_2(\text{gas}) \rightarrow MH_x(\text{solid}) - \Delta E\,, \qquad (2)$$

where

$$\Delta E = E(MH_x) - E(M) - \tfrac{1}{2}xE(H_2)\,, \qquad (3)$$

and $E(MH_x)$ and $E(M)$ are, respectively, the total energies per unit cell of the hydride of concentration $x$ and the pure metal. $E(H_2) = -2.266$ Ry is the Hartree-Fock energy required to separate a hydrogen molecule into its constituent electrons and protons.[35]

The present calculations pertain only to *stoichiometric* hydrides $x = 1$. The reasons for attributing a broader applicability to these results were discussed in Sec. I.

In this section we discuss the hydride heat of formation purely on the basis of one-electron considerations by approximating $E(MH) - E(M)$ by $\Delta E_1$, the difference between the sums of one-electron band energies of the pure metal and the hydride. The contribution of other effects, such as repulsive Coulomb contributions associated with the occupancy of the hydrogen site by more than one electron and strain effects, are estimated in Sec. V.

Detailed calculations of $\Delta E_1$ using band-structure results for the stoichiometric hydrides of Ti, Cr, Mn, Fe, Co, Ni, Cu, Y, Nb, Tc, Ru, Pd, and Ag suggest that $\Delta E_1$ can be represented accurately by the formula

$$\Delta E_1 = 2(\langle \epsilon_{\mathrm{LB}}^{M\mathrm{H}} \rangle - \langle \epsilon_{\mathrm{LB}}^{M} \rangle) + n_d^{M\mathrm{H}}(\langle \epsilon_d^{M\mathrm{H}} \rangle - \langle \epsilon_d^{M\mathrm{H}} \rangle) + \epsilon_F^M . \qquad (4)$$

The first term in Eq. (4) represents the difference in average energy of the lowest band (LB) of the hydride $\langle \epsilon_{\mathrm{LB}}^{M\mathrm{H}} \rangle$ and metal $\langle \epsilon_{\mathrm{LB}}^{M} \rangle$ each of which contains two electrons. The second term describes the shift of the $d$ bands. The quantities $\langle \epsilon_d^M \rangle$ and $\langle \epsilon_d^{M\mathrm{H}} \rangle$ are, respectively, the average energies of the occupied $d$ states lying above LB in the metal and hydride. The average energy of the eleventh electron which occupies the $s$-$d$ hybridized states above the top of the $d$ bands in the noble metals is included in $\langle \epsilon_d^M \rangle$ and $\langle \epsilon_d^{M\mathrm{H}} \rangle$. The quantity $n_d^{M\mathrm{H}}$ is the number of $d$ electrons in the hydride. If the metal has $N_M$ valence electrons, $n_d^{M\mathrm{H}}$ is equal to $N_M - 2$. The $N_M + 1$ electrons per unit cell of the hydride are allocated as follows: two in the lowest band, one at the Fermi level, and $N_d^{M\mathrm{H}}$ in the $d$ bands. Note that the value of $n_d^{M\mathrm{H}}$ is one smaller than the nominal $d$-electron count $N_M - 1$ of a pure transition metal. The third term approximates the contribution of the additional electron per unit cell due to the hydrogen atom which is added on at the Fermi energy $\epsilon_F^M$. Because $\epsilon_F^M$ is referred to an absolute energy scale, $\Delta E_1$ will be sensitive to the choice of the zero of the crystal potential. Since the renormalized-atom method[7,8] has been used to calculate the potentials for all of the hydride systems, this sensitivity should not affect the calculated trends of the heat of formation but it could affect the overall magnitude. One cannot use the metal work function to place the energy levels relative to vacuum because in hydride formation a neutral hydrogen atom passes through the surface and thus the heat of formation is independent of the surface dipole layer contribution to the work function.

When the Brillouin-zone averages in Eq. (4) are evaluated utilizing the ten special points averaging techniques,[22,23] the values of $\Delta E_1$ thus obtained agree to within 0.02 Ry with those resulting from more detailed Brillouin-zone integrations calculations. Equation (4) is therefore seen to be both physically transparent and numerically useful.

The behavior of the three terms of Eq. (4) across the $3d$ and $4d$ rows is illustrated in Figs. 5 and 6, respectively. The plots of the corresponding Wigner-Seitz radii $R_{\mathrm{WS}}$ [Figs. 5(d) and 6(d)] are helpful in understanding the calculated variations. The behavior of $R_{\mathrm{WS}}$ for the transition metals has been discussed by Gelatt *et al.*[8] The initial decrease of $R_{\mathrm{WS}}$ with increasing nuclear charge $Z$ is to be associated with the filling of bonding $d$ orbitals, whereas on the right-hand side of the rows the increase in $R_{\mathrm{WS}}$ is due to the filling of antibonding $d$ orbitals. The overall asymmetry, most clearly exhibited for the $4d$ series in Fig. 6(d), arises from a monotonic reduction of *atomic* size with increasing $Z$.

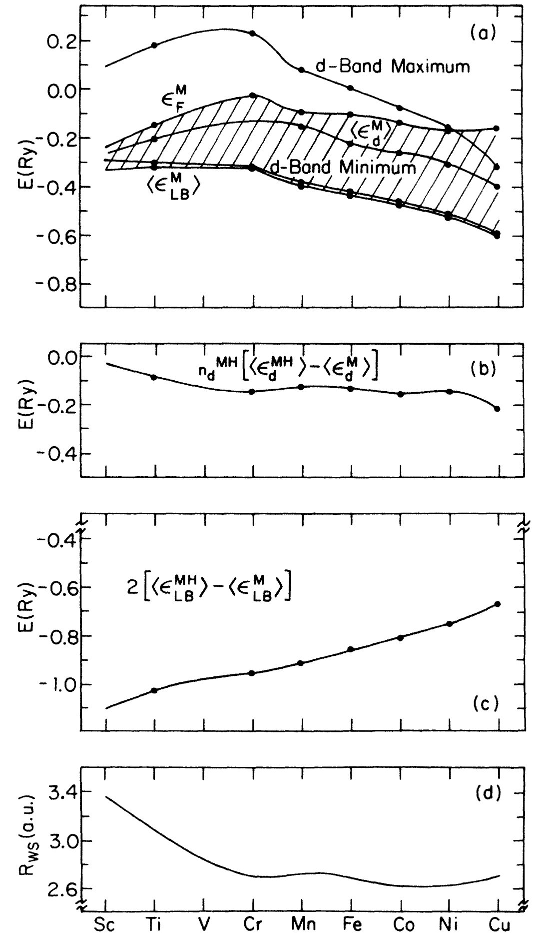

FIG. 5. Variation across the *3d row* of (a) the upper and lower $d$-band edges, the average energy of the occupied $d$ bands $\langle \epsilon_d^M \rangle$, the average energy of the lowest-metal valence band $\langle \epsilon_{\mathrm{LB}}^M \rangle$, and the metal Fermi energy; (b) the shift in energy of the occupied $d$ bands; (c) the occupation-weighted shift in average energy of the lowest band; and (d) the Wigner-Seitz radius $R_{\mathrm{WS}}$.

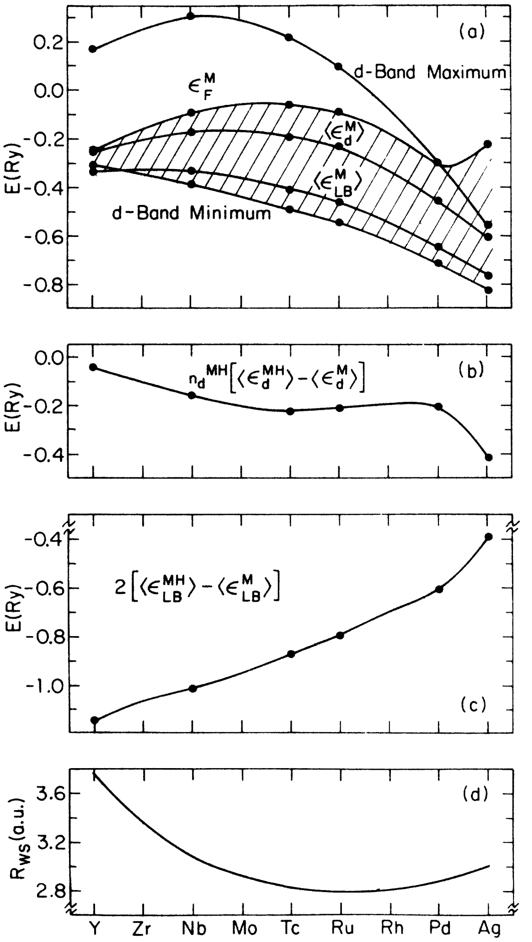

FIG. 6. Variation across the *4d row* of (a) the upper and lower *d*-band edges, the average energy of the occupied *d* bands $\langle\epsilon_d^M\rangle$, the average energy of the lowest metal valence band $\langle\epsilon_{LB}^M\rangle$, and the metal Fermi energy; (b) the shift in energy of the occupied *d* bands; (c) the occupation-weighted shift in average energy of the lowest band; and (d) the Wigner-Seitz radius $R_{WS}$.

Figures 5(a) and 6(a) refer to the pure transition metals. The mean *d*-band energy rises and the bands broaden with decreasing $R_{WS}$ on the left-hand side of the row. The increased energy difference between bonding and antibonding states, respectively, marking the lower and upper *d*-band edges, is due to the greater compression of charge on forming the renormalized atom. This effect is counteracted by the increasing nuclear charge $Z$. Of the two effects, the former dominates on the left-hand side of the row. On the right-hand side, the two effects are in the same direction. Thus, after an initial rise and broadening, the *d* bands shift downwards and become narrower. The behavior of $\epsilon_F^M$ is determined by the preceding effects as well as by increased *d* band filling. The latter is relatively less important for the transition metals on the right-hand side and hence, after rising at the beginning of the period, $\epsilon_F^M$ drops until the *d* bands are completely filled. At this point, $\epsilon_F^M$ enters the relatively low density of states associated with the conduction bands and rises rapidly.

Hydride formation causes the *d* bands to shift downward, as indicated in Figs. 5(b) and 6(b). This shift correlates with the fraction of the charge of these states in the pure metal which has *s* symmetry about the center of the octahedral sites. This charge will sample the hydrogen potential $V_H(r)$ most strongly. The perturbation estimate of Eq. (1) yields a *d*-band shift which to lowest order is proportional to $n_{\rm oct}^s\langle V_H\rangle$, where $\langle V_H\rangle$ is the potential averaged over the octahedral sphere.

The rather weak variation of $\Delta E_d = n_d^{MH}(\langle\epsilon_d^{MH}\rangle - \langle\epsilon_d^M\rangle) = n_d^{MH}\Delta\epsilon_d$ with $Z$, shown in Figs. 5(b) and 6(b), can be understood in terms of the following. In the first half of the period, $\Delta E_d$ results from the energy shift of primarily bonding *d* orbitals. The shift of each bonding *d* orbital is nearly constant because the competing effects of: (a) greater wave-function overlap as $R_{WS}$ decreases; and (b) greater wave-function localization as $Z$ increases, combine to produce a nearly constant amount of octahedral charge and hence a constant energy shift for each bonding level. As a result, the initial slope of $\Delta E_d$ is proportional to $n_d^{MH}$. The increase and change of slope of $\Delta E_d$ occurring after the middle of the period results from two factors. First, the magnitude of each *d*-level shift decreases due to the effects of greater wave-function localization and reduced wave-function overlap associated with, respectively, increasing $Z$ and $R_{WS}$. Secondly, the antibonding *d* states, which have highly localized wave functions, and hence make a small contribution to $\Delta E_d$, are filled in this part of the period. These effects result in a net increase of $\Delta E_d$. The sharp decrease for the noble metals is associated with the lowering of the hybrid *d*-conduction-band states of the sixth band in the hydride, a more important effect in Ag than in Cu.

It is clear from Figs. 5(c) and 6(c) that the nearly linear shift in the average energy of the lowest band is the dominant and most rapidly varying contribution to the heat of formation except for the noble metals. Figure 7, illustrating the average energy of the lowest metal band $\langle\epsilon_{LB}^M\rangle$ and hydride band $\langle\epsilon_{LB}^{MH}\rangle$ for the 3*d* row, shows that the variation of $\langle\epsilon_{LB}^M\rangle$ is three times as great as that of $\langle\epsilon_{LB}^{MH}\rangle$. As a result, the $Z$ dependence of $\langle\epsilon_{LB}^{MH}\rangle - \langle\epsilon_{LB}^M\rangle$ is determined largely by the variation of $\langle\epsilon_{LB}^M\rangle$.

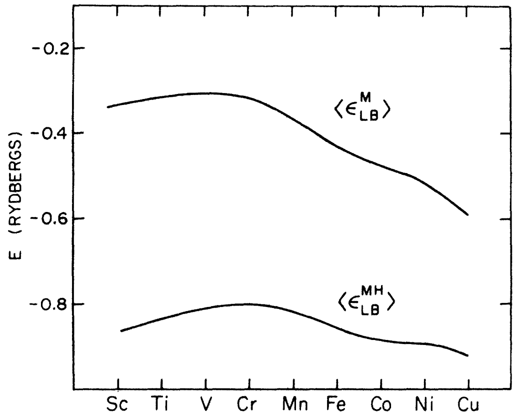

FIG. 7. Variation across the 3*d* row of the average energies of the lowest metal band $\langle\epsilon^{M}_{\mathrm{LB}}\rangle$ and the lowest hydride band $\langle\epsilon^{MH}_{\mathrm{LB}}\rangle$.

The weak $Z$ dependence of $\langle\epsilon^{MH}_{\mathrm{LB}}\rangle$ can be understood qualitatively using a simple model for the alloy in the low-concentration limit. The band results show that in this limit a H-$M$ bonding level forms below the conduction bands whose mean energy is insensitive to hydrogen concentration. We model the potential giving rise to this level by averaging the impurity potential over the metal unit cell, thus forming a dilute substitutional alloy. The energy of the split-off states $\epsilon_{\mathrm{LB}}$ (corresponding to $\langle\epsilon^{MH}_{\mathrm{LB}}\rangle$) is determined by the condition[9]

$$\mathrm{Re}[F_0(\epsilon_{\mathrm{LB}})] = 1/\delta \,, \tag{5}$$

where $F_0(\epsilon) = \langle 0|G(\epsilon)|0\rangle$, $G(\epsilon)$ is the unperturbed host Green's function, $|0\rangle$ refers to a Wannier function associated with cell 0, and $\delta = \epsilon^{\mathrm{H}} - \epsilon_0$ characterizes the strength of the impurity potential. Specifically, $\epsilon_0$ is the mean host metal band energy, and $\epsilon^{\mathrm{H}} = (N_{\mathrm{H}}\epsilon_0^{\mathrm{H}} + N_M\epsilon_0)/(N_{\mathrm{H}} + N_M)$ represents the energy level of the hydrogen-modified unit cell. $N_{\mathrm{H}}$ and $N_M$ are the number of electrons in a muffin-tin sphere associated, respectively, with the hydrogen and metal charge. For the present qualitative purposes it suffices to assume $\epsilon_0^{\mathrm{H}} = -1$ Ry. $\epsilon^{\mathrm{H}}$ thus consists of a weighted average specifying the effectiveness with which an electron samples the hydrogen impurity.

We solve Eq. (5) assuming a simple model for the host density of states $[= -\pi^{-1}\mathrm{Im}F_0(E)]$, shown in Fig. 8 for Cu and Ti which are located roughly at opposite ends of the 3*d* row. In the former case the *d* band is lower and narrower than in the latter. This state density determines $\mathrm{Re}F_0(E)$, and its intersection with the line $\delta^{-1}$, the solution $\epsilon_{\mathrm{LB}}$ of Eq. (5). Figure 8 shows this intersection to occur at about the same energy in the two cases. The near constancy of $\epsilon_{\mathrm{LB}}$ for Cu and Ti is a result of the tradeoff between the magnitude of $\delta$ and the position of the mean energy of the metal band structure. $\epsilon_0$ for Cu is lower than for Ti and $\delta$ is correspondingly weaker. These limited results suggest that $\langle\epsilon^{MH}_{\mathrm{LB}}\rangle$ will be approximately constant across the entire row.

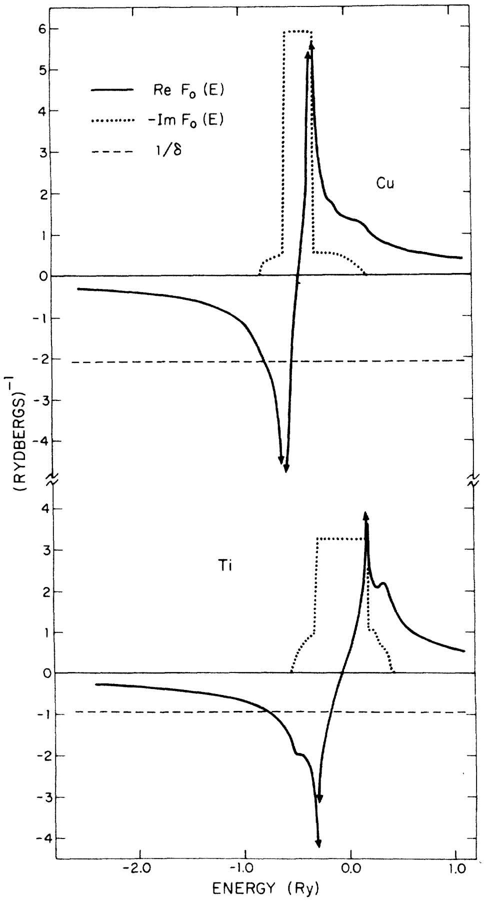

FIG. 8. Plot of the real and imaginary parts of $F_0(E)$ and $\delta^{-1}$ for Cu and Ti. $F_0(E)$ is the trace of the metal Green's function and $\delta$ is the scattering strength of the hydrogen impurity.

To calculate $\Delta E_1$, the metal-related quantities appearing in Eq. (4) should be evaluated using a "touching spheres" metal radius (cf. Sec. II) and the hydride-related quantities using "65–35" radii to better represent the hydrogen site. However, comparisons of band calculations done with both types of radii indicate that the average energy of the individual pure metal *d* bands is 0.02–0.04 Ry lower for the "touching spheres" radius than for the "65–35" radius. Since the lowering of the individual *d* bands in going from the metal to the hydride is of order 0.04 Ry, the hydride *d* band shifts are completely obscured by use of "touching spheres" metal radius for the metal calculations and "65–35" radii for the hydride. As a result,

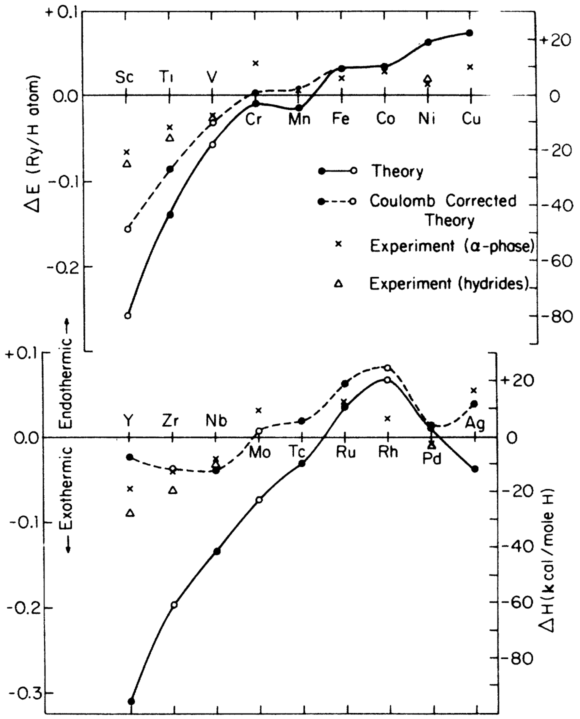

FIG. 9. Calculated heats of formation per hydrogen atom $\Delta E$ for stoichiometric hydrides without (solid line) and with (dashed line) Coulomb energy corrections. The experimental points represent enthalpies of formation of dilute (Ref. 28) and nondilute (Ref. 39) $3d$ and $4d$ hydrides. The open circles indicate elements for which the components of Eq. (4) have been interpolated from those of the neighboring elements.

both $\langle \epsilon_d^M \rangle$ and $\langle \epsilon_d^{MH} \rangle$ were evaluated using "65–35" metal radii.[36] The remaining terms of Eq. (4) which refer to the pure metal were calculated using the "touching spheres" metal radius.

The heats of formation of the stoichiometric $3d$ and $4d$ monohydrides obtained from Eqs. (4) and (3) are shown in Fig. 9.[37] These calculations used the equilibrium Wigner-Seitz radius of the pure metal since much of the existent experimental data pertains to dilute hydrides where lattice-expansion effects are negligible. The points representing $\Delta E$ for Ti, Cr, Mn, Fe, Co, Ni, Cu, Y, Nb, Tc, Ru, Pd, and Ag were obtained by calculating the components of Eq. (4) directly from the band-structure results. Those representing Sc, V, Zr, Mo, and Rh are the result of interpolating values of $\langle \epsilon_{LB}^M \rangle$, $\langle \epsilon_{LB}^{MH} \rangle$, $\langle \epsilon_d^M \rangle$, $\langle \epsilon_d^{MH} \rangle$, and $\epsilon_F^M$. For the noble metals, it was necessary to modify Eq. (4) by substituting for $\epsilon_F^M$ the explicit energy $(\sim \epsilon_F^{MH})$ at which the extra electron is added. This modification is required because for these metals the hydride Fermi energy can be substantially lower than the pure-metal Fermi energy, a consequence of the lowering of the upper conduction-band states in the hydride. These states are occupied only in the noble metals.

In the absence of systematic studies of monohydrides, we show in Fig. 9 a collection of experimental points for dilute hydrogen solutions[38] and nondilute hydrides.[39]

In view of the approximations made here, comparisons between theory and experiments should be limited to an examination of general trends across the periods. The gross features of the $\Delta E$ curve reflect the general experimental situation, namely, that with the exception of Pd and Ni stable concentrated hydrides form only on the left-hand sides of the period. The results shown in Figs. 5 and 6 indicate that the shape of the solid curve is determined by the variation with $Z$ of both the Fermi energy and the lower band shift. The large magnitude of the latter in the first part of each period is responsible for the associated relatively large formation energies. The drop in the theoretical curve near Pd and the shoulder near Co are attributable to the $Z$ dependence of the Fermi energy shown in Figs. 5 and 6. Although $\beta$-phase palladium hydride is stable at room temperature and pressure, its heat of formation is very small compared to that of the hydrides of Y and Ti and when viewed on the scale of the hydrogen dissociation energy, 1.13 Ry. The characteristic weak binding of PdH is also evident from the theoretical curve for $\Delta E$, even though the computed value of $\Delta E$ is slightly positive. The experimentally observed increase in binding of hydrogen by the metal near Ni in the $3d$ row is not reproduced by the calculations. Comparing the behavior of the Fermi level in the $3d$ and $4d$ rows, shown in Figs. 5(a) and 6(a), one observes that the difference is the result of the bands dropping less rapidly with increasing nuclear charge in the $3d$ row. It should be noted that the calculated $d$ band width for Ni is almost 2 eV larger than that observed in photoemission experiments,[34] a problem which is unique to Ni.

A comparison of the computed and experimental values of $\Delta E$ for the early transition metals (and Ag) indicates that the one-electron calculation overestimates the stability of these hydrides. This results from a neglect of the Coulomb energies arising from the presence of more than one electron on a H site. Corrections associated with these effects are estimated in Sec. V. The calculated heats of formation including the corrections are indicated by the dashed curves in Fig. 9.

## V. CORRECTIONS TO BAND RESULTS

This section will deal with the hydrogen Coulomb energy resulting from occupancy of a hydrogen

TABLE IV. Integrated muffin-tin sphere charge for the metal site in the pure metal, the metal hydride, and their difference; the integrated muffin-tin sphere charge for the hydrogen site in the pure metal, the metal hydride, their difference, and the lattice constant used in the calculations. The "65–35" prescription is used for the muffin-tin radius.

| | Ti | Cr | Fe | Ni | Cu | Y | Nb | Ru | Pd | Ag |
|---|---|---|---|---|---|---|---|---|---|---|
| $N_{\mathrm{MT}}^{M}(M)$ | 2.80 | 4.53 | 6.57 | 8.76 | 9.85 | 1.82 | 3.42 | 6.31 | 8.74 | 9.82 |
| $N_{\mathrm{MT}}^{M}(M\mathrm{H})$ | 2.76 | 4.64 | 6.74 | 8.95 | 9.95 | 1.61 | 3.39 | 6.40 | 8.76 | 9.79 |
| $\Delta N_{\mathrm{MT}}^{M}$ | −0.04 | +0.11 | +0.17 | +0.19 | +0.10 | −0.21 | −0.02 | +0.09 | +0.01 | −0.03 |
| $N_{\mathrm{MT}}^{\mathrm{H}}(M)$ | 0.22 | 0.28 | 0.27 | 0.22 | 0.21 | 0.26 | 0.32 | 0.30 | 0.21 | 0.20 |
| $N_{\mathrm{MT}}^{\mathrm{H}}(M\mathrm{H})$ | 1.14 | 1.04 | 0.98 | 0.89 | 0.98 | 1.45 | 1.22 | 1.08 | 1.00 | 1.17 |
| $\Delta N_{\mathrm{MT}}^{\mathrm{H}}$ | +0.92 | +0.76 | +0.71 | +0.67 | +0.77 | +1.19 | +0.90 | +0.78 | +0.79 | +0.97 |
| $a$ (a.u.) | 7.81 | 6.83 | 6.78 | 6.61 | 6.77 | 9.77 | 7.82 | 7.12 | 7.32 | 7.67 |

site by more than one electron, an effect which has not been considered in the estimate of the hydride heat of formation based on $\Delta E_1$.

For convenience, we shall monitor the amount of charge associated with the hydrogen site by considering the charge contained in the relevant muffin-tin sphere. While it would clearly be better to define a more realistic hydrogen sphere radius, perhaps in analogy with the Wigner-Seitz radius associated with the metal atom, it is difficult to define this radius unambiguously.[40] Table IV indicates that the amount of charge contained in the hydrogen muffin tin is greater than unity for some systems. The question arises whether this effect is to be associated with charge transfer from the metal to the hydrogen site or can be accounted for in some other way.

There is much speculation in the hydride literature on the nature of the chemical bond between hydrogen and metal atoms.[1,2] Although there is no conclusive experimental evidence, it is argued that in the hydrides of the early transition metals some of the metal charge is transferred to hydrogen, thereby producing a partially ionic bond. Estimates of charge transfer based on the present calculations are complicated not only by the difficulties associated with partitioning the charge in the unit cell, but also by the accuracy with which the average charge decompositions are computed. The accuracy of the present calculations is such that the total charge contained in metal and hydrogen muffin tins, respectively, is estimated to be correct to about 0.05 electrons. Since the charge transfer effects themselves are likely to be of that order, we cannot arrive at an unambiguous view as to whether charge transfer effects are indeed important. While not excluding the presence of charge transfer except possibly in the case of early-period metals and Ag, it will be argued that the charge densities contained in the two muffin-tin spheres can be accounted for without invoking the notion of charge transfer. The results shown in Table IV are useful in this respect. By inspecting the changes in total charge contained in the metal muffin-tin sphere and the octahedral site in a metal upon forming the hydride, it appears that the metal is acquiring charge at the expense of the hydrogen in the middle of the rows in contrast to the prevailing views that the charge transfer is in the opposite direction. This effect can be explained without invoking interatomic charge transfer by recalling that on hydride formation an electron is transferred from the lower metal band to the Fermi energy, that is, from a diffuse bonding state to a localized antibonding state. The metal $d$-charge density thus becomes more localized and more charge is contained within the metal muffin-tin radius. This viewpoint is consistent with the fact that $\Delta N_{\mathrm{MT}}^{M}$ increases across the rows to Ni and Pd. The effect, however, is not present for Cu and Ag, where the $d$ bands are already filled in the pure metal and the transferred electron lies in the conduction-band complex. That $\Delta N_{\mathrm{MT}}^{M}$ is less than zero for Ti, Y, Nb, and Ag indicates that charge transfer may be important in these hydride systems.

The behavior of the quantities $\Delta N_{\mathrm{MT}}^{M}$ and $\Delta N_{\mathrm{MT}}^{\mathrm{H}}$ can also be explained by invoking an intuitive argument to the effect that the charge present in the hydrogen muffin-tin radius can be represented approximately as

$$\rho(r)=\rho_0+\alpha\rho_{\mathrm{H}}(r)\,, \tag{6}$$

where $\rho_0$ is the average charge density in the octahedral sphere in the pure metal, and $\rho_{\mathrm{H}}(r)=\pi^{-1}e^{-2r}$ is the charge density of a free hydrogen atom. In the present context, $\alpha$ is to be interpreted as a

TABLE V. Components of the calculation of the Coulomb energy correction. The rows contain the hydrogen-site muffin-tin radius, the average charge density in the hydrogen-site sphere in the pure metal, the fraction of the charge of a hydrogen atom contained in a sphere of radius $R^{\mathrm{H}}_{\mathrm{MT}}$, the parameter $\alpha$ from Eq. (6), the Coulomb integral defined by Eq. (8), and the Coulomb energy correction given by Eq. (7).

| | Ti | Cr | Fe | Ni | Cu | Y | Nb | Ru | Pd | Ag |
|---|---|---|---|---|---|---|---|---|---|---|
| $R^{\mathrm{H}}_{\mathrm{MT}}$ (a.u.) | 1.37 | 1.20 | 1.19 | 1.16 | 1.19 | 1.71 | 1.37 | 1.25 | 1.28 | 1.34 |
| $\rho_0$ (el. a.u.$^{-3}$) | 0.020 | 0.039 | 0.038 | 0.035 | 0.030 | 0.013 | 0.030 | 0.037 | 0.023 | 0.020 |
| $N_{\mathrm{H}}$ | 0.51 | 0.43 | 0.42 | 0.41 | 0.42 | 0.66 | 0.52 | 0.45 | 0.47 | 0.50 |
| $\alpha$ | 1.80 | 1.76 | 1.68 | 1.64 | 1.83 | 1.79 | 1.74 | 1.72 | 1.68 | 1.93 |
| $F^0$ (Ry) | 0.65 | 0.59 | 0.53 | 0.46 | 0.54 | 0.88 | 0.73 | 0.62 | 0.52 | 0.70 |
| $\Delta E$ (Ry) | 0.05 | 0.01 | 0.0 | 0.0 | 0.0 | 0.29 | 0.10 | 0.03 | 0.0 | 0.07 |

renormalization parameter. The appropriateness of this argument rests on whether the calculated charge density can indeed be fit by this parametrized expression across the entire row for a constant value of $\alpha$. Table V shows that this is true to fair approximation. Figure 10 illustrates the parametrized form. The approximate validity of this superposition again suggests that it is possible to account for the increased charge around the proton without invoking a significant amount of charge transfer.

The increased charge associated with each proton does lead to a repulsive Coulomb energy which decreases the heat of formation. The neglect of this effect in $\Delta E_1$ is predominantly responsible for the discrepancy between theory and experiment on the left-hand side of each row. We shall estimate this effect by assuming that the charge to be associated with each proton is that contained in the hydrogen muffin-tin sphere and by adopting a band theoretic viewpoint within the spin-restricted Hartree-Fock approximation which postulates that the occupany of spin-up and spin-down states is the same. Within the context of a Hubbard-like approach, these Coulomb energies result from the repulsion between spin-up and spin-down electrons. We approximate the associated energy by the expression

$$\Delta E = \tfrac{1}{2} N_{\mathrm{H}}(N_{\mathrm{H}} - 1)F^0 , \qquad (7)$$

where $N_{\mathrm{H}}$ is the charge ascribed to the hydrogen sphere and $F^0$ is the Slater-Coulomb integral evaluated in the muffin-tin sphere

$$F^0 = \int\int \rho_\sigma(\vec{r}_1)\,\frac{2}{r_>}\,\rho_{-\sigma}(\vec{r}_2)\,d\vec{r}_1\,d\vec{r}_2 . \qquad (8)$$

The charge density $\rho_\uparrow(r) = \frac{1}{2}\rho(r)$ is the charge associated with spin-up electrons, $\rho_\downarrow$ that associated with spin-down electrons, and $\rho(r)$ is the total charge density. The factor of $\frac{1}{2}$ in Eq. (7) is introduced to prevent double counting of the electron-electron interaction. We observe that this expression reduces correctly to the Hubbard result in the case of a nondegenerate filled band and vanishes if the band is half occupied. The results for the range $1 < N_{\mathrm{H}} < 2$ depend on the model chosen and would differ from those suggested by Eq. (7) in an unrestricted Hartree-Fock viewpoint. They should suffice, however, to exhibit the trends that we are trying to explain in connection with Fig. 9. Table V presents the results of the calculation of $\Delta E$ for the $3d$ and $4d$ metal hydrides. Because of the larger values of $N^{\mathrm{H}}_{\mathrm{MT}}$ on the left-hand side of the periods, the hydrogen associated Coulomb energies are larger there and diminish as one proceeds to the right across the row. The addition of these corrections to the heats of formation calculated from one-electron energy differences, shown by the dashed curve in Fig. 9, is seen considerably to improve the agreement of the calculated heats of formation with experiment.

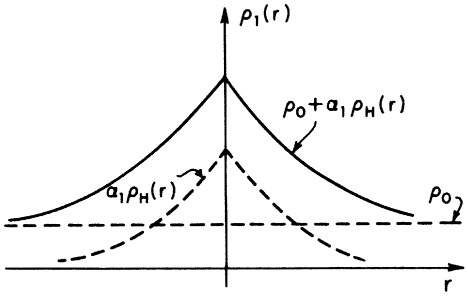

FIG. 10. Schematic representation of the decomposition of the hydrogen charge density (solid curve) into a constant metal component $\rho_0$, and an atomic hydrogen component $\rho_{\mathrm{H}}(r)$ scaled by the factor $\alpha$ (dashed curve).

The Coulomb correction given by Eq. (7) is a rough correction for the lack of charge self-consistency in the present calculations. In cases such as Y and Nb, where the correction is large on the scale of the calculated heat of formation, this simple estimate of the Coulomb correction is less reliable. It might also be argued that the large Coulomb energies of the early transition metals are conducive to polyhydride formation which is characteristic of that part of the transition-metal rows since the inclusion of more than one proton per unit cell can be shown to reduce the Coulomb penalty because fewer electrons are associated with each proton.[17]

## ACKNOWLEDGMENTS

The authors would like to thank Professor G. W. Pratt, Jr. and Dr. H. L. Davis for supplying computer codes for the band calculations, Dr. W. R. Wampler and Dr. B. Lengeler for informing us of the $\mathrm{CuH}_x$ Dingle-temperature results prior to publication, and Dr. K. Kritayakirana who assisted in the early stages of these calculations. L. Huisman and E. Esposito provided computational assistance and helpful comments. This work was supported in part by the National Science Foundation through Grant Nos. DMR72-02977 and DMR76-01111.

## APPENDIX A: TWO ATOM PER UNIT CELL AVERAGE *t*-MATRIX APPROXIMATION

The derivation of the average $t$-matrix approximation (ATA) for a muffin-tin model of an alloy with more than one atom per unit cell follows that for the single atom per cell case.[9] The single-particle Hamiltonian in atomic units is

$$H=p^2+\sum_n \sum_i V_n^i(\vec{r}). \tag{A1}$$

Atoms are located at $\vec{R}_n+\vec{\tau}_i$, where $\vec{R}_n$ denotes a crystal lattice vector and $\vec{\tau}_i$ a basis vector within a unit cell. The potentials $V_n^i(\vec{r})$ are assumed to be spherically symmetric and to vanish for $|\vec{r}|>R_{\mathrm{MT}}^i$, the muffin-tin radius for atoms at the $i$th site within a cell.

The equilibrium properties of the alloy are most conveniently discussed in terms of the configuration averaged single-particle Green's function

$$G(E)=\langle (E-H)^{-1}\rangle, \tag{A2}$$

where $\langle \cdots \rangle$ here and in the following denotes configuration averaging over the occupation of the sublattice sites. It is convenient to introduce the average total-scattering operator $T(E)$, which is related to $G(E)$ by

$$G=G_0+G_0TG_0, \tag{A3}$$

where $G_0$ is the free-particle Green's function. $T$ can be expressed in terms of $t_n^i$, the atomic scattering matrices, which are related to the single-site potentials by

$$t_n^i=V_n^i(1-G_0V_n^i)^{-1}. \tag{A4}$$

The resulting multiple scattering series for $T$ is

$$T=\sum_{n,i}\langle t_n^i\rangle+\sum_{\substack{n,i\\ n',i'\neq n,i}}\langle t_n^i G_0 t_{n'}^{i'}\rangle+\cdots. \tag{A5}$$

Neglecting fluctuations in the average, the central approximation of the ATA, allows one to replace the average of products by products of averages. Equation (A5) becomes

$$T=\sum_{n,i}\langle t_n^i\rangle+\sum_{\substack{n,i\\ n',i'\neq n,i}}\langle t_n^i\rangle G_0\langle t_{n'}^{i'}\rangle+\cdots, \tag{A6}$$

where, if sublattice $i$ consists of atoms $A$ and $B$ with concentrations $x$ and $1-x$,

$$\langle t_n^i\rangle = x t^{A(i)}+(1-x)t^{B(i)}. \tag{A7}$$

Equation (A5) has the same form as the equation for the total scattering operator of a pure crystal with a basis with effective atomic scattering matrices $\langle t_n^i\rangle$. The multiple scattering series in Eq. (A6) can be summed in an angular momentum representation. The momentum representation of the atomic $t$-matrices has the form

$$\langle \vec{k}|t^A|\vec{k}'\rangle=(4\pi)^2\sum_L Y_L(\vec{k})t_l^A(k,k')Y_L(\vec{k}').$$

Just as in a pure crystal, the complex energy bands, i.e., the locus of poles of the diagonal matrix elements of $T$ in the momentum representation, depend only on the energy-shell matrix elements of $t^i$ (the case $|\vec{k}|=|\vec{k}'|=E^{1/2}=\kappa$) which can be expressed in terms of the phase shifts $\eta_l^{A(i)}, \eta_l^{B(i)}$, of the single-site potentials. For example,

$$t_l^{A(i)}(\kappa,\kappa)=-\kappa^{-1}e^{i\eta_l(\kappa)}\sin[\eta_l(\kappa)]. \tag{A8}$$

Following the crystalline derivation,[41] the complex energy bands are determined by the condition

$$\| i\kappa\langle \cot[\eta_l^i(\kappa)]\rangle \delta_{LL'}^{ii'}+A_{LL'}^{ii'}(\vec{k},\kappa)\|=0, \tag{A9}$$

where

$$\kappa\langle \cot[\eta_l^i(\kappa)]\rangle=-\langle t_l(\kappa,\kappa)\rangle^{-1}+i\kappa, \tag{A10}$$

and the $A_{LL'}^{ii'}$ are the KKR structure factors for a "complex" crystal, extended here to complex energies. The matrix in Eq. (A9) is not Hermitian (except for $\kappa^2$ real and negative), thus the eigenenergies are complex.

## APPENDIX B: DETAILS PERTAINING TO THE HEAT-OF-FORMATION CALCULATIONS

The calculations of the heat of formation of metal hydrides reported in Sec. IV are, to our knowledge, the first systematic attempt to calculate heats of formation for an entire family of compounds. A number of parameters, such as the lattice constant, muffin-tin radii, and the muffin-tin zero of the potential had to be selected without the benefit of prior experience. We have not attempted to optimize the choice of these parameters, rather we chose one convenient scheme (described in Sec. II) for selecting them and used it systematically for all calculations. In this Appendix we discuss checks of the sensitivity of the results to the choice of parameters.

### A. Lattice constant

The density of metal atoms in the stable metal hydrides is usually less than that in the pure metal. Since our calculations included systems which do not form stable hydrides, we chose to use the same density for both the metal and the metal hydride rather than to guess the most favorable density for each system. Calculations have been carried out for TiH, NiH, and CuH with the lattice constant expanded by 5.6%. The qualitative effects of increasing the lattice constant are: (i) the metal *d* bands narrow and become more tightly bound, thus approaching the case of the isolated atom; (ii) the Fermi energy, which rides the *d* band, drops; (iii) the sixth band, primarily a conduction band, falls, reflecting the decreased kinetic energy due to the reduced electronic density; and (iv) the bottom band lowering between the metal and the metal hydride is reduced because the *d* bands in the metal fall more rapidly than the metal-hydrogen level in the hydride. The heats of formation of the hydrides calculated from the electronic energies in the expanded lattice metal and expanded lattice metal hydride using the methods of Sec. IV are greater (more exothermic) by 0.014, 0.061, and 0.069 Ry/(unit cell) for TiH, NiH, and CuH, respectively. To this difference should be added the energy cost of expanding the pure metal lattice which can be calculated from the bulk modulus of the metal. The net result is an increase in the strength of the binding of the expanded lattice hydride relative to the normal lattice hydride of 0.001, 0.046, and 0.058 Ry/(unit cell), consistent with the observed decrease in metal density which accompanies hydride formation in these systems.

### B. Muffin-tin radii

The calculated heat of formation is quite sensitive to the relative sizes of the metal and hydrogen muffin-tin spheres. The calculations in Sec. IV used the "touching spheres" (see Sec. II) muffin-tin radius for the pure metal (but the "65–35" prescription for the metal *d*-band average energy), and the "65–35" prescription for the hydride. A calculation of the heat of formation using touching spheres for both Pd and PdH gives $\Delta E_1 = -0.94$ Ry/(unit cell) compared to $-1.13$ Ry/(unit cell) used in Sec. IV. A calculation using the "65–35" radii for both Pd and PdH yields $\Delta E_1 = -1.22$ Ry/(unit cell). Reducing the size of the hydrogen sphere, as in the touching spheres prescription, reduces the binding of the metal-hydrogen level by 0.06 Ry, and increases the binding of each of the metal *d* bands by about 0.02 Ry in both the metal and the hydride so the effect on $\langle \Delta\epsilon_d \rangle$ is small. Using the "65–35" prescription for the pure metal results in a less tightly bound lowest band, thus increasing the lowering of the bottom band when the hydride is formed, and increasing the heat of formation.

The damping of the bands in the nonstoichiometric hydrides is also affected by the size of the hydrogen muffin-tin sphere. The Fermi-surface damping calculations in Sec. III used the touching spheres prescription. Using the "65–35" prescription decreases the damping by about 25%. The change is essentially independent of the nature of the state. Thus, the shape of the curves representing the Fermi-surface damping in Fig. 4 would not be affected by using the "65–35" prescription, but the magnitude would be in poorer agreement with experiment.

### C. Shifts in the Muffin-tin zero

The potential in the region between the muffin-tin spheres was assumed to be the same in the metal hydride as in the pure metal for lack of an easily implemented calculation of its shift when the proton is added to a unit cell. A calculation for CuH with a depressed muffin-tin zero verifies the expectation of first-order perturbation theory: the shift of a one-electron level $\delta\epsilon_i$ when the muffin-tin zero is shifted by $\delta V_{\mathrm{MT}}$ can be approximated as $\delta\epsilon_i = n_i^{\mathrm{PW}}\delta V_{\mathrm{MT}}$, where $n_i^{\mathrm{PW}}$ is the fraction of the charge density of the state which resides in the intersphere region. This expression is found to be accurate to within about 5%. One expects $V_{\mathrm{MT}}$ to be more negative in the hydride than in the pure metal because an attractive potential has been added to the unit cell. If it is assumed that this shift in $V_{\mathrm{MT}}$ is the same for all elements in a period, the resulting increase in the binding of the hydride will be proportional to the total amount of charge in the intersphere volume in the hydride. This quantity is of order 1.1 electrons per unit cell for Ti and Cu and increases to 1.35 electrons per unit cell in the center of the row. Thus, a 0.1-Ry decrease in $V_{\mathrm{MT}}$ would result in a uniform increase in hydride binding of about 0.1 Ry, but trends would be affected very little.

[1] W. M. Mueller, J. P. Blackledge, and G. G. Libowitz, *Metal Hydrides* (Academic, New York, 1968), Chap. 6.

[2] G. G.Libowitz, *The Solid State Chemistry of Binary Metal Hydrides* (Benjamin, New York, 1965), Chap. 1.

[3] Y. Ebisuzaki and M. O'Keeffe, Prog. Solid State Chem. 4, 187 (1967); J. Phys. Chem. 72, 4695 (1968).

[4] The screened proton model predicts a maximum in the binding energy of a hydride for every maximum in the Fermi-level density of states. Electronic heat-capacity data [C. Kittel, *Introduction to Solid State Physics,* 4th ed. (Wiley, New York, 1971), p. 254] thus predicts peaks for 3, 5, 7, and 9 electrons per atom in the $3d$ and $4d$ transition-metal rows.

[5] A. C. Switendick, Solid State Commun. 8, 1463 (1970); Int. J. Quantum Chem. 5S, 459 (1971); Ber. Bunsenges. Phys. Chem. 76, 535 (1972).

[6] J. C. Slater, *The Self-Consistent Field for Molecules and Solids: Quantum Theory of Molecules and Solids,* Vol. 4 (McGraw-Hill, New York, 1974), Chap. 1.

[7] L. Hodges, R. E. Watson, and H. Ehrenreich, Phys. Rev. B 5, 3953 (1972).

[8] R. E. Watson and H. Ehrenreich, Comments Solid State Phys. 3, 109 (1970); C. D. Gelatt, Jr., H. Ehrenreich, and R. E. Watson, Phys. Rev. B 15, 1613 (1977).

[9] H. Ehrenreich and L. M. Schwartz, in *Solid State Physics,* edited by H. Ehrenreich, F. Seitz, and D. Turnbull (Academic, New York, 1976), Vol. 31, p. 149; A. Bansil, H. Ehrenreich, L. Schwartz, and R. E. Watson, Phys. Rev. B 9, 445 (1974).

[10] D. E. Eastman, J. K. Cashion, and A. C. Switendick, Phys. Rev. Lett. 27, 35 (1971).

[11] J. Jacobs, R Griessen, F. D. Manchester, and Y. de Ribaupierre, Bull. Am. Phys. Soc. Ser. II 21, 409 (1976).

[12] W. R. Wampler and B. Lengeler, Phys. Rev. B 15, 4614 (1977).

[13] J. A. Weiss, C. D. Gelatt, and H. Ehrenreich, Bull. Am. Phys. Soc. Ser. II 20, 420 (1975).

[14] Reference 1, Chap. 10.

[15] D. G. Pettifor, J. Phys. C 3, 367 (1970).

[16] The formation energies of hydrides do not vary appreciably with the structure and concentration of the hydride. For example, the enthalpy of formation of tetragonal $\epsilon$-phase ZrH$_2$ is $-38.9$ kcal/(mole H); the enthalpy of formation of cubic $\delta$-phase ZrH$_{1.5}$ is $-33.7$ kcal/(mole H). Plots of the hydrogen partial enthalpy of formation of hydrides which form over a wide concentration range also indicate that the heat of formation per hydrogen atom is a slowly varying function of hydrogen concentration (see Refs. 1 and 2).

[17] J. A. Weiss, Ph.D. thesis (Harvard University, 1975) (unpublished).

[18] The Hartree-Fock wave functions used for the heat-of-formation calculations are $d^{n-1}s$ average of configuration results. For Nb and Ag the wave functions are from J. B. Mann, Los Alamos Scientific Report Nos. LA-3690, 1967, LA-3691, 1968 (unpublished). For Ti, Cr, Mn, Fe, Co, Ni, Cu, Y, Tc, Tu, and Pd the wave functions were calculated using the MCHF72 program [C. Froese-Fischer, Comput. Phys. Commun. 4, 107 (1972)]. The nonstoichiometric PdH$_x$ calculations used frozen-core wave functions based on analytic-core wave functions for Pd$^+$ ($d^9$) [R. E. Watson (unpublished)].

[19] E. C. Snow and J. T. Waber, Acta Metall. 17, 623 (1969).

[20] The program used for our calculations was a modified version of the MIT program by J. H. Wood, L. F. Mattheiss, and A. C. Switendick.

[21] J. Korringa, Physica 13, 392 (1947); W. Kohn and N. Rostoker, Phys. Rev. 94, 1111 (1954).

[22] A. Baldereschi, Phys. Rev. B 7, 5212 (1973).

[23] D. J. Chadi and M. L. Cohen, Phys. Rev. B 8, 5747 (1973).

[24] L. Hodges, Ph.D. thesis (Harvard University, 1966) (unpublished); H. Ehrenreich and L. Hodges, Methods Comput. Phys. 8, 149 (1968).

[25] Reference 17 includes results for NaCl structure hydrides of Ti, Cr, Fe, Ni, Cu, Nb, and Pd.

[26] F. A. Lewis, *The Palladium/Hydrogen System* (Academic, New York, 1967).

[27] J. S. Faulkner, Phys. Rev. B 13, 2391 (1976).

[27] (a) J. Zbasnik and M. Mahnig, Z. Phys. B 23, 15 (1976). The augmented-plane-wave virtual-crystal approximation is an inadequate model for the electronic structure of alloys for two reasons: (i) The calculated energy bands are real when in fact the disorder will lead to damping of the states (i.e., complex eigenvalues). (ii) The weight of a filled band in a nonstoichiometric compound $AB_x$ is two (including spin) even if the state is localized on $B$ atoms. When applied to PdH$_x$ the method leads to the unreasonable result that the magnitude of the density of states of the split-off metal-hydrogen bonding level (plotted in Fig. 4) is essentially independent of hydrogen concentration.

[28] F. M. Mueller, A. J. Freeman, J. O. Dimmock, and A. M. Furdyna, Phys. Rev. B 1, 4617 (1970).

[29] The present calculations yield $d$ bands which are 0.09 Ry broader and 0.02 Ry closer to the bottom of the conduction band than those found using an $X\alpha$ potential for a $d^9s$ configuration by Mueller *et al.* (Ref. 28). For PdH with the lattice constant $a = 7.6157$ a.u. the renormalized-atom $d$ bands are 0.02 Ry broader, and the metal-hydrogen bonding band is about 0.1 Ry farther below the Fermi level than found by Switdendick (Ref. 5) using an $X\alpha$ potential.

[30] L. Huisman (personal communication).

[31] B. Velicky, S. Kirkpatrick, and H. Ehrenreich, Phys. Rev. 175, 747 (1968).

[32] L. Huisman and J. A. Weiss, Solid State Commun. 16, 983 (1975).

[33] The experimental values are from Ref. 12. The theoretical values are the results of Ref. 32 corrected for electron-phonon enhancement using the values of $\lambda(\vec{k})$ published by M. J. G. Lee, Phys. Rev. B 2, 250 (1970).

[34] D. E Eastman, in *Electron Spectroscopy,* edited by D. A. Shirley (North-Holland, Amsterdam, 1972), p. 487.

[35] W. Kolos and C. C. J. Roothaan, Rev. Mod. Phys. 32, 219 (1960).

[36] A calculation of $d$ band shifts for equilibrium lattice constant Pd indicates that the same magnitude of $d$ band shift is obtained using "touching spheres" muffin-tin radii for both the metal and the hydride as was found using the "65–35" prescription.

[37] The present calculations differ from those in a preliminary report of this work [C. D. Gelatt, Jr., J. A. Weiss, and H. Ehrenreich, Solid State Commun. 17, 663 (1975)] primarily because of the use of ten rather than two special point integrations for obtaining Brillouin-zone averages of band energies. In addition, an error in the calculation for Ag has been corrected.

[38] R. B. McLellan and W. A. Oates, Acta Metall. 21, 181 (1973).

[39] The nondilute hydrides shown are $ScH_2$, $TiH_{1.61}$, $VH_{0.50}$, $NiH_{0.5}$, $YH_2$, $ZrH_2(\epsilon)$, $NbH_{0.67}$, and $PdH_{0.56}$. The values are from Ref. 1.

[40] Attempts to define such an effective hydrogen sphere radius are discussed in Ref. 17, Sec. 4.

[41] B. Segall, Phys. Rev. 105, 108 (1957).

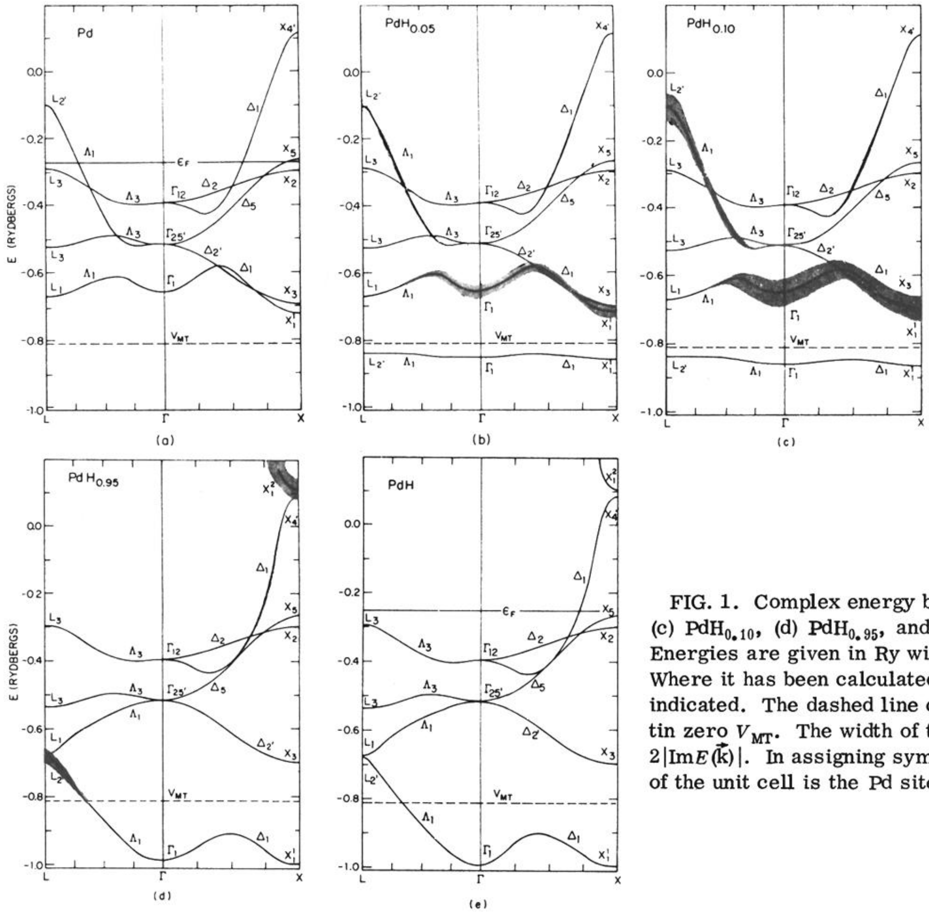

FIG. 1. Complex energy bands of (a) Pd, (b) $PdH_{0.05}$, (c) $PdH_{0.10}$, (d) $PdH_{0.95}$, and (e) PdH along $\Lambda$ and $\Delta$. Energies are given in Ry with respect to vacuum. Where it has been calculated, the Fermi energy $\epsilon_F$ is indicated. The dashed line corresponds to the muffin-tin zero $V_{MT}$. The width of the shading corresponds to $2|\mathrm{Im}E(\vec{k})|$. In assigning symmetry labels, the origin of the unit cell is the Pd site.